Synthesis of layered double hydroxides with nitrate and its adsorption properties of phosphate

Jiangpo Zhang, Qi Xia, Xiaofeng Hong, Jianjun Chen and Daijun Liu

ABSTRACT

In the present study, different ratios of layered double hydroxides (LDHs) were synthesized via co-precipitation method. The synthesized LDHs were characterized by Fourier transform infrared spectroscopy (FT-IR), X-ray diffraction (XRD), nitrogen adsorption-desorption analysis, point of zero charges (pH_{pzc}), scanning electron microscopy (SEM) and transmission electron microscopy (TEM). Phosphate adsorption performances were estimated by batch adsorption experiments; desorption hysteresis and adsorption mechanism were also investigated. The XRD, SEM and TEM results confirmed the multilayer structure of the synthesized LDHs. The pseudo-second-order kinetic model and the Freundlich model describe the adsorption behavior of LDHs best. The maximum adsorption capacity is 185.86 mg-KH_2PO_4/g for Mg_2Al-NO_3 LDH. When the dosage of LDHs was greater than 2 g/L, the phosphorus content in the solution decreased from 30 mg-P/L to 0.077 mg-P/L after adsorption by Mg_2Al-NO_3 LDH. All the results reveal that Mg_2Al-NO_3 LDH is a potential adsorbent for removing phosphate from aqueous solution.

Key words | adsorbent, adsorption kinetic, layered double hydroxide, phosphate adsorption

Jiangpo Zhang
Qi Xia
Xiaofeng Hong
Jianjun Chen (corresponding author)
Daijun Liu
School of Chemical Engineering,
Sichuan University,
Chengdu 610065,
China
E-mail: *chenjianjun@scu.edu.cn*

Jianjun Chen
Daijun Liu
Engineering Research Center for Comprehensive Utilization and Cleaning Process of Phosphate Resource,
Ministry of Education,
Chengdu 610065,
China

HIGHLIGHTS

- Layered double hydroxides were successfully prepared with nitrate by the co-precipitation method.
- The layered structure can be seen from the SEM and TEM image.
- The synthesized LDHs can significantly reduce the content of phosphate in water.

INTRODUCTION

Phosphorus is a non-renewable resource and is an indispensable element that is essential for the growth of organisms on our planet. However, wastewater containing a considerable quantity of soluble phosphate is discharged into waters, which results in eutrophication and subsequent deterioration of lakes, lagoons, rivers, and sea (Valsami-Jones 2005). Eutrophication has become one of the most severe problems in aquatic environments. It causes algal blooms and consumes the dissolved oxygen in the water (Alshameri *et al.* 2014). Thus, removing phosphorus from wastewater is the key to solving the problem. Various methods have been developed to remove phosphate from contaminated water, such as chemical precipitation (Liu *et al.* 2019), crystallization (Li *et al.* 2016b), biological process (Law *et al.* 2016). Chemical precipitation requires many expensive flocculants or coagulants, and the resulting sludge is prone to secondary pollution (Zhang *et al.* 2012a). The biological process is unstable and difficult to control because dephosphorization efficiency is greatly affected by the quality of water. Adsorption is a promising method to remove phosphate from the polluted water due to its cost-effective, environmentally friendly, and reliable operation (Lalley *et al.* 2016).

Layered double hydroxides (LDHs), also known as bimetallic hydroxides, is a multi-functional anionic clay that has been attracted considerable research attention due to its excellent adsorption ability to anions, unique properties, and applications such as catalysts, pharmaceuticals,

doi: 10.2166/wst.2020.567

ion-exchange materials, and drug storage-delivery agents (Zhang *et al.* 2013). The general chemical formula that best characterizes LDHs is $[M^{2+}_{1-x}M^{3+}_{x}(OH)_2]^{x+}(A^{n-})_{x/n}{\cdot}mH_2O$, where M^{2+} represents a divalent metal cation, M^{3+} represents a trivalent metal cation, A^{n-} are the incorporated anions in the interlayer space, x is the molar ratio of $M^{3+}/(M^{2+}+M^{3+})$, and m is the number of water molecules. The structure of LDHs consists of positively charged brucite-like layers with trivalent cations partially substituting for divalent cations, and the excess positive charges are balanced by exchangeable compensating anions and water molecules, as seen in Figure 1. Strong chemical bonds within the layers and relatively weak bonds between interlayer anions and layers make LDHs promising ion-exchangers for anions. Hence, LDHs have been investigated to absorb inorganic and organic anion pollutants from water, such as arsenate, molybdate, selenite, fluoride, and nitrate (Hatami *et al.* 2018; Zhang *et al.* 2019).

Numerous studies have been conducted to focus on the synthesis process with low-cost and readily available materials (Kong *et al.* 2019), structure characterization (Zhang *et al.* 2012b), and its application to remove the heavy metals as adsorbent (Zhao *et al.* 2020), and application as a catalyst carrier (Dewangan *et al.* in press). However, there were few studies investigating the removal of phosphate by LDHs. Therefore, the objectives of the present study were to focus on the effect on the properties of LDHs synthesized with different ratios and investigate the performance of synthesized LDHs for phosphate removal from wastewater and figure out the factors that affect the adsorption process.

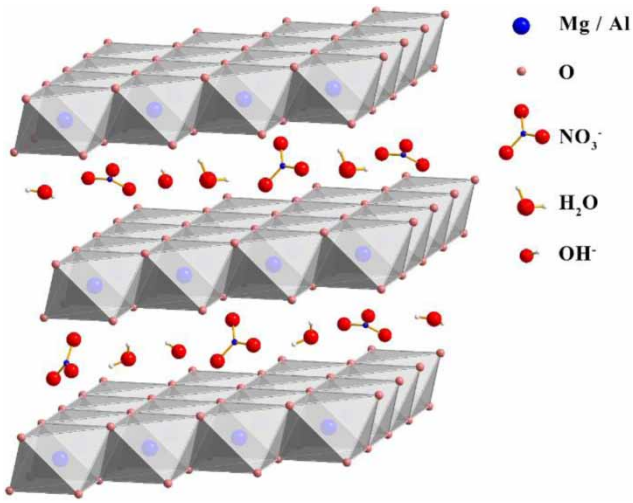

Figure 1 | The layered structure of LDHs.

MATERIAL AND METHODS

Synthesis of LDHs

All the chemicals used in this study were analytical grade and purchased from Kelong Chemical Co. Ltd (Sichuan, China). The Mg-Al LDHs were synthesized via the co-precipitation method. The aqueous NaOH (1.0 mol/L) and the mixed nitrate solution containing Mg $(NO_3)_2{\cdot}6H_2O$ and Al $(NO_3)_3{\cdot}9H_2O$ of Mg/Al at a preset molar ratio (2:1, 3:1, 4:1) were simultaneously added dropwise into a three-necked flask until the value of pH reached 10. The resulting slurry was aged at 80 °C for 6 h in a water bath. The precipitate was filtered, washed with deionized water several times, and subsequently dried at 80 °C for 12 h. Finally, the obtained samples were ground into 40–100 mesh and stored in sample bottles for further use. The samples were labeled as $Mg_xAl\text{-}NO_3$, where x represents the Mg/Al molar ratio.

Characterizations

The Fourier transform infrared spectroscopy (FT-IR) was used to analyze the functional group of the sample from 4,000 cm^{-1} to 500 cm^{-1} on a Nicolet Avatar 370DTGS spectrophotometer (Thermo Fisher Scientific, USA). X-ray diffraction (XRD) analysis was carried out to identify any crystallographic structure in the samples using a computer-controlled X-ray diffractometer (Cu Kα radiation, Philips Electronic Instruments, USA) equipped with a stepping motor and graphite crystal monochromator. The specific surface area and pore volume were calculated using the Brunauer-Emmett-Teller (BET) method, and the pore size distribution was analyzed form the desorption branch isotherms using Barrett-Joyner-Halenda (BJH) analysis. The morphologies and element distribution of the samples were characterized using scanning electron microscopy (SEM, FEI Inspect F50) and energy-dispersive spectroscopy (EDS) mapping analysis. Transmission electron microscopy (TEM) was determined with LIBRA 200 FE (Zeiss, Germany). The content of metal ions of the as-prepared samples and the concentration of dissolved metal ions in different pH after phosphate adsorption were analyzed by an inductively coupled plasma-mass spectrometry (ICP-OES).

Adsorption and desorption studies

For the kinetics of phosphate adsorption, a phosphate solution (50 mg-P/L) was prepared by dissolving K_2HPO_4 in

deionized water. The experiments were carried out as follows: 0.1 g of adsorbent was added into a 500 mL conical flask containing 200 mL phosphate solution with a stirring speed of 120 rpm at room temperature. The supernatant was extracted at different time intervals and filtered through a 0.45 μm membrane filter. The phosphorus concentration in the supernatant was measured by UV spectrophotometry at 700 nm using the molybdenum-blue ascorbic acid method (Yan *et al.* 2018). The phosphate uptake was calculated from the decreases in phosphate concentration regarding those of the initial solution. The amount of phosphate retention on per unit mass of LDHs was computed using the formula:

$$q_e = \left(\frac{(C_i - C_e)V}{m}\right) \times 1000 \quad (1)$$

where q_e is the phosphate uptake (mg-K_2HPO_4/g-LDHs), C_i is the initial concentration (mg/L), C_e is the final equilibrium concentration (mg/L), V is the volume of the solution (L), and m is the mass of the adsorbent (g).

The adsorption isotherms of phosphate were conducted under different temperatures (20, 30 and 40 °C) with 50 mL phosphate solution and 50 mg adsorbent, the initial phosphate concentration varied from 50 to 600 mg-KH_2PO_4/L and the pH value of the solution was 7, then the solution with adsorbent was stirred at a speed of 120 rpm at room temperature for 24 h, and the phosphate adsorption capacity and the concentration at equilibrium were measured.

For the study of the desorption ability of LDHs, first, phosphate saturated LDHs (P-LDHs) were achieved by mixing an appropriate dosage of LDHs with a 50 mg-P/L K_2HPO_4 solution for 24 h, then the phosphate capacity was calculated by Equation (1). Then, a series of KOH solutions were utilized as eluant to desorb the P-LDHs. The phosphorus content in the eluate was measured by UV spectrophotometry at 700 nm using the molybdenum-blue ascorbic acid method. The desorption rate was estimated from the following equations:

$$Desorption\ Rate(\%) = \frac{Q_{des}}{Q_{ads}} \times 100 \quad (2)$$

where Q_{ads} is the amount of phosphate uptake in the adsorption operation (mg-K_2HPO_4/g-LDHs), and Q_{des} is the amount of phosphate desorbed in the desorption operation (mg-K_2HPO_4/g-LDHs).

The desorption isotherm also investigated the effect of adsorption-desorption hysteresis. After the adsorption isotherm experiment, a half volume of the supernatant was immediately sampled for phosphate concentration measurement, then 25 mL KOH solution with a mass concentration of 20% was supplemented to allow desorption for another 24 h, then the phosphate adsorption capacity and the concentration were determined.

RESULTS AND DISCUSSION

Characterization of LDHs

In order to determine the chemical composition of the prepared adsorbents, the FT-IR spectra of synthesized LDHs are shown in Figure 2(a). The broad band between 3,445 ~ 3,480 cm^{-1} and the weak peak near at 1,630 cm^{-1}

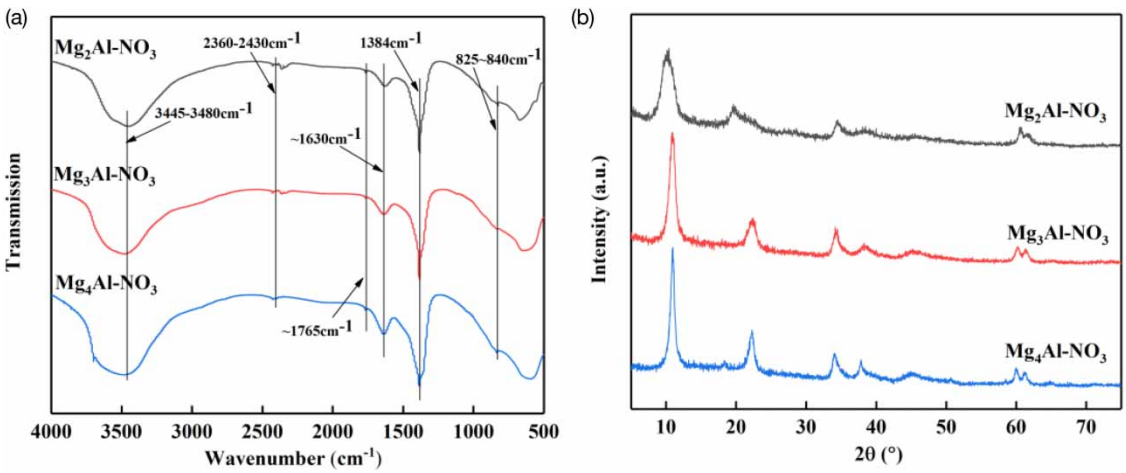

Figure 2 | The FT-IR spectra (a) and XRD patterns (b) of different LDHs.

in the spectra of all the prepared LDHs were attributed to the O-H stretching vibrations of the OH group in the brucite-like layer, and the H-O-H is the bending vibration of the water molecule in the interlayer (Shi *et al.* 2020), respectively. The strong band at 1,384 cm^{-1} corresponds to the stretching vibration of the nitrate ion (Mohamed *et al.* 2018), the weak bands between 826–840 cm^{-1} were also caused by nitrate ions. The bands observed for carbonyl groups at 1,765 cm^{-1} and between 2,360–2,430 cm^{-1} were related to the CO_2 background of the measurement system. Additionally, the bands between (400 cm^{-1} to 800 cm^{-1}) correspond to the lattice vibrations of M-O, M-O-M, and O-M-O (where M are metal ions) (Juboury 2019).

The XRD patterns of synthesized LDHs are shown in Figure 2(b). All the samples exhibit the typical characteristic reflections of the hydrotalcite structure. The typical reflections of 003 planes (9.9–10.4°) and 006 planes (19.9–20.6°) at lower 2θ, the 012 planes at ~34–35° 2θ, and the 110 planes at higher ~60–62° 2θ indicate a well-formed layered structure (Bao *et al.* 2020). With the increase of the Mg/Al ratio, the peak of (003) plane of the LDHs becomes sharper and shifts to higher 2θ values, which mean that the samples are better crystallized. However, the basal space decreased owing to the decreased positive charge density. Some lattice parameters of reflection were calculated by Bragg diffraction formula and are summarized in Table 1. The d_{003} corresponds to the basal space of the unit layer, the constant a is the cation-cation distance in the brucite-like layer, which was calculated from $a = 2d_{110}$, and $c = 3d_{003}$ is related to the thickness of the brucite-like layers and interlayer space. The interlayer space was computed by subtracting the brucite-like sheet thickness, which is 4.8(Å), as confirmed in many articles (Everaert *et al.* 2016; Zhang *et al.* 2019) from the basal space d_{003}. The parameter a also increased with the increase of the Mg/Al ratio, which conforms with the report (Zhang *et al.* 2019).

The N_2 adsorption-desorption isotherm of the different LDHs are presented in Figure S1 (Supplementary Material). The curves of all the samples belonged to the type-IV isotherm model with H4 type hysteresis loops resulting from capillary condensation according to IUPAC classification (Hu *et al.* 2018). The BJH desorption plots of volume desorbed versus pore diameter are presented in the insets in Figure S1. The pore size distribution of all the samples lay between 2–20 nm, demonstrating the existence of mesopores. The specific surface area, average pore diameter, and total pore volume are summarized in Table 2. The specific surface area decreased due to the high crystallinity with the increasing metal ratio in the samples. The positive charge density of the lamellar decreased with the increasing metal ratio, resulting in a decrease of the interaction between metal ions; hence, the pore volume decreased.

The point of zero charge is the concentration of potential-determined ions in solution when the charge on the surface of the material is zero. The potential-determined ions in solution of the experiment are hydrogen ions and hydroxyl ions. The pH of the point of zero charge pH_{pzc} is the pH value of the solution when the charge on the surface of material is zero and this was measured by the pH drift method (Santos *et al.* 2019). Briefly, the pH of 50 mL NaCl (0.01 mol/L) solution was adjusted between 2 and 12 with 1 mol/L HCl or NaOH solution. The adsorbents (0.1 g) was added to the solution, and stirred at room temperature for 6 h, and the final pH was recorded. Figure S2 shows the graphs of final versus initial pH to determine the points at which the initial pH and final pH values were equal. The points were taken as the pH_{pzc} of the adsorbents, and the data are listed in Table 3. The pH_{pzc} increases with the increase of the Mg/Al ratio; as the metal ratio increases, the surface positive charge density of the material decreases, and only a small amount of hydroxide ions are needed to make the surface charge density of the material equal to zero, then the pH of the solution is high; hence, the

Table 1 | XRD data of diffraction peaks and the lattice parameters of LDHs

LDHs	d_{003} (Å)	d_{110} (Å)	$a = 2\ d_{110}$ (Å)	$c = 3\ d_{003}$(Å)	interlayer space (Å)
Mg_2Al-NO_3	8.929	1.526	3.052	26.787	4.129
Mg_3Al-NO_3	8.114	1.537	3.074	24.342	3.314
Mg_4Al-NO_3	8.094	1.540	3.080	24.282	3.294

Table 2 | The pore textural characteristics of LDHs

LDHs	Surface area (m^2/g)	Average pore size (nm)	Pore volume (cm^3/g)
Mg_2Al-NO_3	67.6	15.3	0.245
Mg_3Al-NO_3	32.0	3.2	0.127
Mg_4Al-NO_3	9.1	3.2	0.025

Table 3 | The molar Mg/Al ratio in material and pH_{pzc} of different LDHs

LDHs	Molar Mg/Al ratio in material	pH_{pzc}	Adsorption capacity (mg-KH_2PO_4/g)
Mg_2Al-NO_3	2.03	7.82	185.86
Mg_3Al-NO_3	2.91	8.42	122.98
Mg_4Al-NO_3	3.63	9.97	110.39

measured pH_{pzc} becomes higher. According to the point of zero charges, the adsorbent surface has a positive charge when $pH < pH_{pzc}$, the adsorption of anions is favored at the pH values lower than pH_{pzc}.

The SEM images of as-synthesized LDHs and LDHs after adsorption are shown in Figure 3. It can be seen that the prepared $Mg_2Al\text{-}NO_3$ LDH has an apparent layered structure and is superimposed layer by layer to form

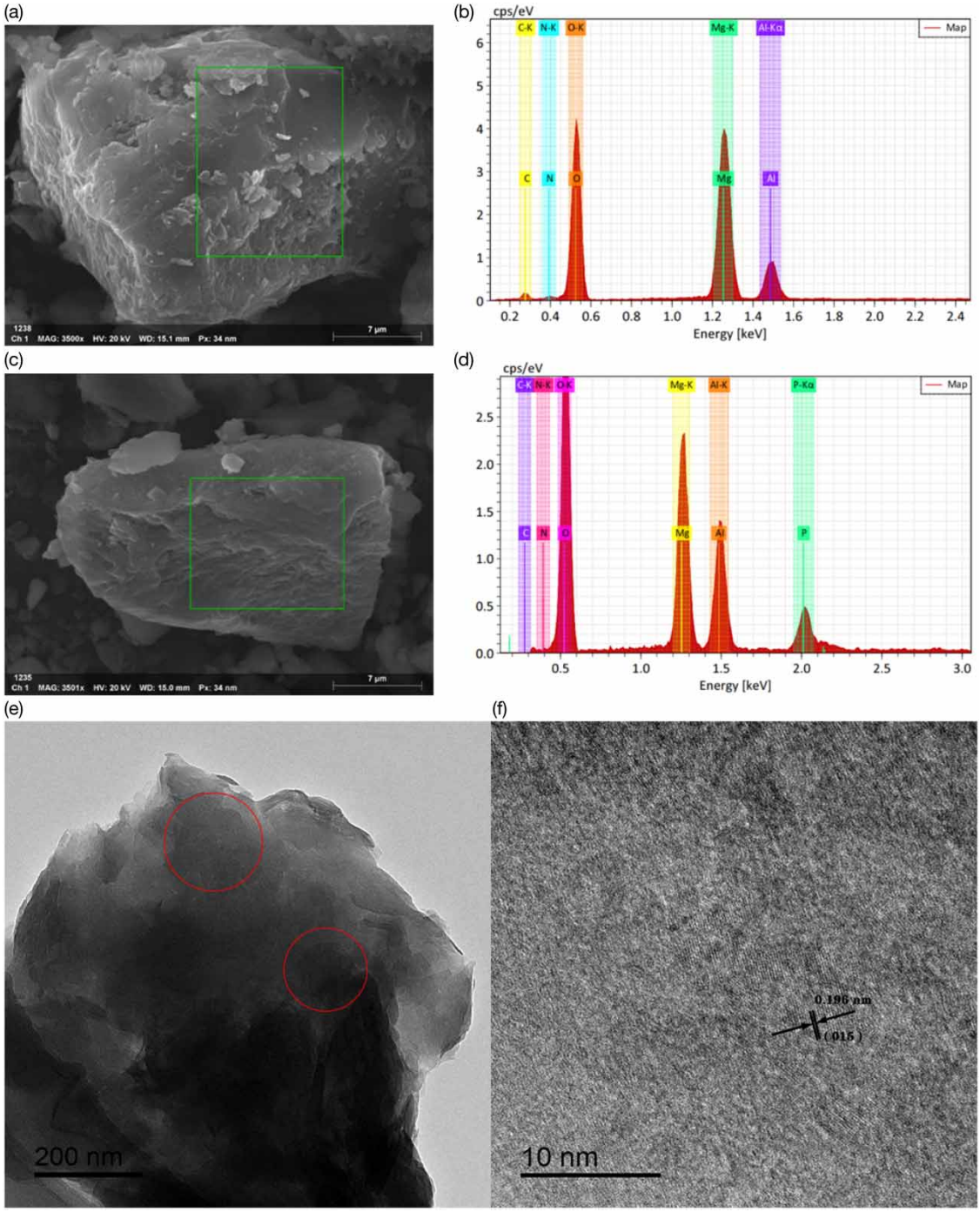

Figure 3 | Images of (a) as-synthesized $Mg_2Al\text{-}NO_3$ LDH, (b) EDS analysis of as-synthesized $Mg_2Al\text{-}NO_3$ LDH, (c) $Mg_2Al\text{-}NO_3$ LDH after adsorption, (d) EDS analysis of $Mg_2Al\text{-}NO_3$ LDH after adsorption, (e) and (f) the HRTEM of as-synthesized $Mg_2Al\text{-}NO_3$ LDH.

particles (Figure 3(a) and 3(c)). The HRTEM image also confirmed the characteristic morphology of multilayer structure form with hexagonal, plate-like particles (Figure 3(e)), which is consistent with the paper (Abukhadra *et al.* 2020a). It was found that the crystal particle structure with interplanar spacing is about 0.196 nm (Figure 3(f)), which is in agreement with the data determined from the XRD result (the spacing of (015) plane is 0.199 nm). The results of the EDS spectra of Mg_2Al-NO_3 LDH before adsorption confirmed that the samples consisted of oxygen, magnesium, aluminum, and nitrogen (Figure 3(b)). From the EDS analysis of the Mg_2Al-NO_3 sample after phosphate adsorption (Figure 3(d)), the presence of phosphorus can be seen, which is due to the exchange of phosphate with nitrate. The details can be seen in the section, Adsorption mechanism).

Batch adsorption and desorption studies

Effect of contact time on the phosphate adsorption

The results of equilibrium phosphate adsorption on the different Mg-Al LDHs are shown in Figure S3. The data show that the phosphate uptake rapidly exceeds half of the equilibrium adsorption capacity in the first 2 hours, then increases slowly till the equilibrium is reached. The equilibrium adsorption capacity of LDHs decrease with the decrease of metal ratio, as can be seen from Table 3. The reason seems to be evident that the adsorption capacity is significantly related to the interlayer space. The larger the basal space is, the easier is ion exchange, and the more phosphate is adsorbed. Everaert *et al.* (2016) computed the size of the phosphate ion and the geometrical result showed that the height of the phosphate ion in the interlayer is between 3.38 and 3.86 Å; the interlayer space of the prepared samples can be seen from Table 1, Mg_2Al-NO_3 has the largest interlayer space of 4.129 Å and its phosphate adsorption capacity is 185.86 mg-KH_2PO_4/g. The interlayer spaces of Mg_3Al-NO_3 and Mg_4Al-NO_3 are below 3.38 Å, indicating that the anions in the interlayer can hardly be exchanged by phosphate ions. Namely, the phosphate adsorption capacity of the two LDHs will be lower than Mg_2Al-NO_3.

Adsorption kinetic

Three models were employed to investigate the adsorption mechanisms of LDHs on phosphate. Figure 4(a)–4(c) show the fitting results of the pseudo-first-order model, pseudo-second-model, and intraparticle diffusion model respectively. The equations are documented in the Supplementary Material. The fitting parameters for the three models are presented in Table 4. The correlation

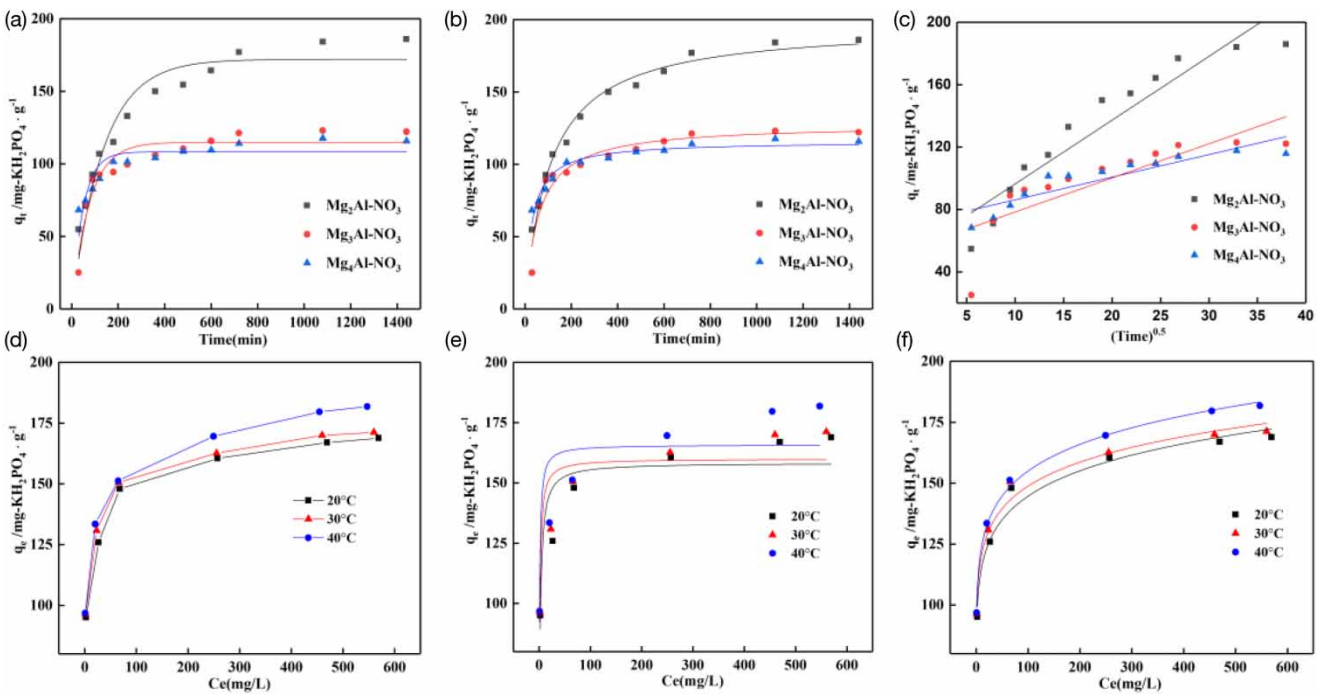

Figure 4 | The fitting results of different kinetics of phosphate adsorption onto different LDHs and the adsorption isotherm results of Mg_2Al-NO_3 LDH: (a) pseudo-first-order model; (b) pseudo-second-order model; (c) intraparticle diffusion model; (d) adsorption isotherm plots; (e) Langmuir model; (f) Freundlich model.

Table 4 | Kinetic models for phosphate adsorption on samples and the calculated constants

	Pseudo-first-order				Pseudo-second-order				Intraparticle diffusion			
LDHs	q_e	k_1	R^2	SSE	q_e	k_2	R^2	SSE	k_i	C_i	R^2	SSE
$Mg_2Al\text{-}NO_3$	171.99	0.00748	0.923	1,514	196.66	4.78×10^{-5}	0.982	348	1.450	71.68	0.793	2,299
$Mg_3Al\text{-}NO_3$	114.91	0.01316	0.897	783	127.66	1.36×10^{-4}	0.918	624	2.187	56.48	0.629	2,820
$Mg_4Al\text{-}NO_3$	108.29	0.02068	0.724	753	115.87	2.97×10^{-4}	0.930	190	4.091	55.43	0.884	564

coefficient (R^2) represents the concordance degree between the experimental and predicted values by the suggested models. Ranging between 0 and 1, R^2 close to 1 confirms that the model has a high concordance between the actual and predicted values. The discrepancy of the data can be measured using sum of squared errors (*SSE*) (Abdul-Hameed & Al Juboury 2020). The equilibrium adsorption capacity of the pseudo-second-order kinetic fitting was close to the experimental value. The higher R^2 and lower *SSE* of the pseudo-second-order than those of the other two kinetics indicated that the pseudo-second-order model fits the phosphate adsorption on the LDHs better, suggesting the adsorption process is primarily dominated by chemisorption (Abukhadra *et al.* 2020b). The intraparticle diffusion model was also taken into account to find out whether it is a rate-limiting factor in the adsorption process. The fitting curves of intraparticle diffusion did not fit well, and the correlation coefficient R^2 was the least of the three, indicating that intraparticle diffusion was not the critical step of the adsorption process.

Adsorption isotherm and thermodynamic

The results of phosphate adsorption isotherms on $Mg_2Al\text{-}NO_3$ are shown in Figure 4(d). It is obvious that the adsorption capacity increased with increase of both the temperature and the phosphate concentration, indicating that the adsorption process was endothermic. The adsorption isotherm under different temperatures was also simulated by Langmuir and Freundlich models and their illustrative equations are documented in the Supplementary Material, the results are shown in Figure 4(e) and 4(f), and the relevant isotherm parameters can be seen in Table 5. The Freundlich model performed better prediction for the adsorption processes due to its higher R^2 and lower *SSE* comparing with the Langmuir isotherm model. The thermodynamic parameter Gibbs free energy (ΔG°) was calculated using the following equation:

$$\Delta G^\circ = -RT \ln K^\circ \tag{3}$$

where R is the constant of perfect gas (R = 8.314 J/mol·K), T is the absolute temperature of solution (K), and K° is the standard equilibrium constant.

The value of the enthalpy (ΔH°), and the entropy (ΔS°) were determined from the linear regression curves of $1/T$ vs $\ln(K)$ based on the Van't Hoff equations (Figure S4) (Abukhadra & Mostafa 2019):

$$\ln(K) = \frac{\Delta S^\circ}{R} - \frac{\Delta H^\circ}{RT} \tag{4}$$

As seen in Table 5, the negative value of ΔG° indicates spontaneity of the adsorption process and as the temperature increased, the free energy became more negative indicating that the adsorption became more favorable at higher temperature. The positive enthalpy indicated that the process is endothermic and the positive value of ΔS° suggested an increased degree of freedom in the system and indicated high affinity of the $Mg_2Al\text{-}NO_3$ adsorbent with phosphate.

Table 5 | Theoretical parameters of Langmuir model, Freundlich model, and thermodynamic studies

	Langmuir				Freundlich						
Temperature (K)	q_{max}	K_L	R^2	SSE	1/N	K_F	R^2	SSE	ΔG° (J mol^{-1})	ΔH° (J mol^{-1})	ΔS° (J K^{-1} mol^{-1})
293.15	158.31	0.538	0.765	779	0.100	91.09	0.966	115	−22,808	31,466	185.4
303.15	160.02	0.895	0.764	792	0.093	97.02	0.973	94	−24,896		
313.15	165.83	1.169	0.692	1,317	0.099	98.19	0.996	17	−26,505		

Effect of pH on the phosphate adsorption

The pH of the solution is one of the essential parameters for the phosphate adsorption. It can change the surface charge of LDHs and the form of phosphate in aqueous solution. The experiment was conducted in a 100 mL conical flask containing 50 mg adsorbent and 50 mL KH_2PO_4 solution (the concentration was 50 mg-P/L). The initial pH of the solution was adjusted to about 2, 4, 6, 8, 10, and 12 with 1 mol/L HCl or NaOH solution, then the conical flask was oscillated at ambient temperature for 24 h, and the phosphate adsorption capacity was calculated and is shown in Figure 5(a). For the LDHs with Mg/Al = 2 and 3, the phosphate adsorption capacity increases with the increase in pH when the pH value is below 6, then decreases with the increase in pH value. The adsorption capacity was high for $Mg_4Al\text{-}NO_3$ when the pH was 2, this may be because the dissolved metal ions interact with the phosphate and form insoluble precipitates. The concentration of dissolved elements Mg and Al in the solution after adsorption were also measured, the results are shown in Figure S5, and specific data can be seen in Table S1 and Table S2 (Supplementary Material). More than 60% of magnesium was dissolved into the solution at pH 2 of all the LDHs, then the amount of dissolved magnesium decreased below 5% until the pH increase to 8. About 15% of the aluminum dissolved at pH 2 of $Mg_2Al\text{-}NO_3$ and $Mg_3Al\text{-}NO_3$. However, less than 5% of the aluminum dissolved at pH 2 of the LDHs with Mg/Al = 4, and the solution became cloudy after adsorption, which confirmed the formation of insoluble phosphates. Aluminum also dissolved somewhat at pH 12 because of its amphoteric property. To determine the optimal pH range of the adsorbents, taking the metal solubility and pH_{pzc} into account, the optimal adsorption pH range of different samples are from pH = 7 to pH_{pzc}.

Effect of the dosage on the phosphate adsorption

The adsorption experiment of a solid-liquid ratio was carried out to investigate whether the phosphorus content in the solution treated with LDHs could meet the national industrial discharge standard. A series of adsorbents ($Mg_2Al\text{-}NO_3$) of different dosages were added to the conical flask containing 50 mL KH_2PO_4 solution (30 mg-P/L) stirred for 24 h at room temperature. The final phosphorus content of the solution was measured, and the result is shown in Figure 5(b). The final phosphorus content is below 0.077 mg-P/L when the solid-liquid ratio is greater than 2 g/L, indicating that $Mg_2Al\text{-}NO_3$ is a very effective adsorbent treating phosphorus aqueous solution.

Desorption and desorption hysteresis

It is essential to investigate the desorption ability of saturated phosphorous adsorbent for the phosphate recovery. As seen in Figure S6, when the desorption time is 12 h, only KOH with a mass concentration of 15% can achieve a desorption rate of 95%. Nevertheless, the desorption rate is more than 95% after desorption for 18 h when the mass concentration of KOH is no less than 10%. Therefore, KOH with a mass concentration of 10% was used as a desorption agent, and the desorption time was 18 h. The results of the desorption experiments of different LDHs are shown in Figure 6. The desorption rate decreased slightly with the

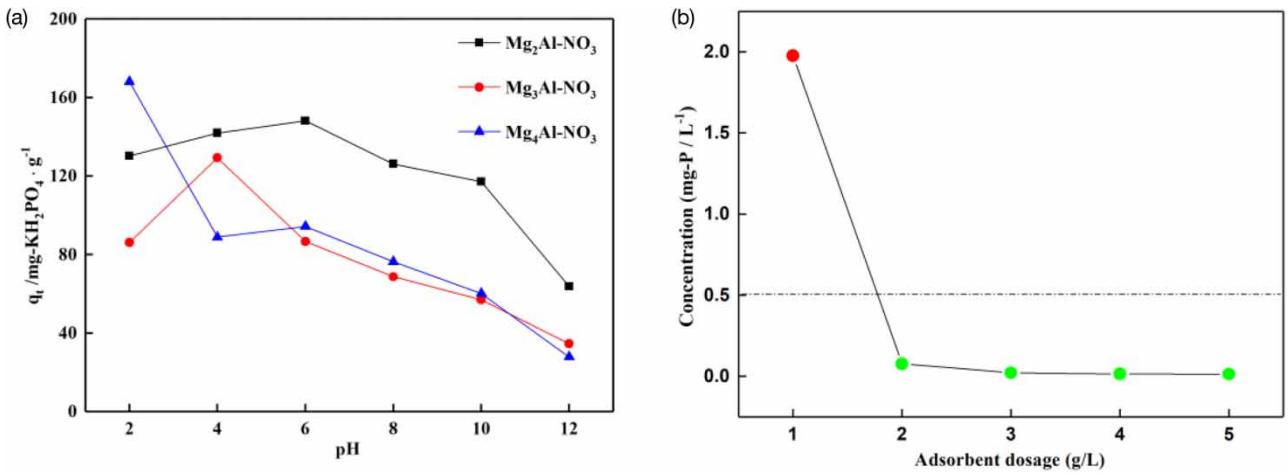

Figure 5 | (a) Effect of pH on the phosphate adsorption capacity of different LDHs; (b) effect of adsorbent dosage on the phosphorus concentration in the solution after adsorption by $Mg_2Al\text{-}NO_3$ LDHs.

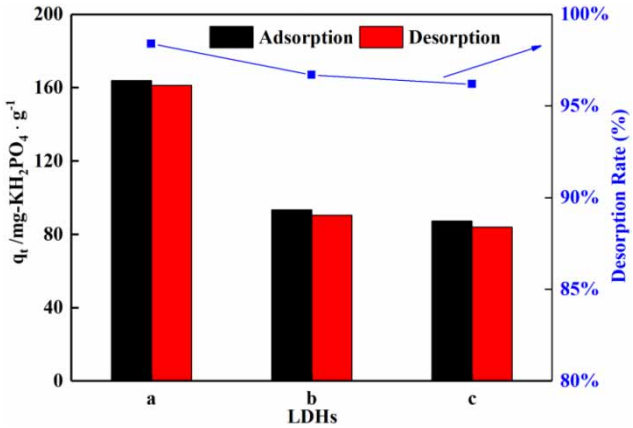

Figure 6 | The desorption of different LDHs: (a) Mg_2Al-NO_3, (b) Mg_3Al-NO_3, (c) Mg_4Al-NO_3.

increase in the Mg/Al ratio, but all the samples showed good desorption efficiency, and the desorption rate was all above 95%. It showed that KOH with a mass concentration of 10% is a suitable eluent. The desorption isotherm data of Mg_2Al-NO_3 at 30 °C was also simulated by Freundlich model (Figure S7), the results are presented in Table S3, The $K_{F,des}$ and $1/N_{des}$ values represent the desorption capacity and desorption intensity respectively (Adeola & Forbes 2020). The H value is defined as the ratio of the $1/N$ to $1/N_{des}$ and higher H values indicate more desorption hysteresis, no desorption hysteresis occurs when $H = 0$. The H value of this study is 0.284, which suggest that slight adsorption-desorption hysteresis occurred. The hysteresis may have been caused by the formation of insoluble precipitation and incomplete ion exchange during the adsorption process.

Adsorption mechanism

The phosphate adsorption mechanism is complicated and was studied based on the characterization results before and after phosphate adsorption of the Mg_2Al-NO_3 adsorbent. As shown in Figure S8(a), the band at 1,384 cm^{-1} originating from the stretching vibration of the nitrate ion became weaker and the weak bands between 826–840 cm^{-1} disappeared after the phosphate adsorption; the new band at 1,063 cm^{-1} after adsorption represents the stretching vibration of P-O in phosphate. The change was attributed to the exchange of nitrate ions with phosphate ions (Kong *et al.* 2019). Further evidence about phosphate adsorption by Mg_2Al-NO_3 adsorbent was obtained from the XRD analysis (Figure S8(b)). After phosphate adsorption, the reflection intensity of (003) plane decreased but the structure of Mg_2Al-NO_3 LDH remained, this is consistent with the SEM results before and after phosphate adsorption. The decreased reflection intensity of the (003) plane, probably due to the ligand complexation between phosphate (which acts as a ligand) and metal ions on the surface of the LDH layer and the formation of insoluble precipitates caused by the dissolved metal with phosphate during the ion exchange process (Everaert *et al.* 2016). The XRD pattern showed a double (006) plane reflection, indicating the presence of two different anion species in the interlayer (nitrate and phosphate), which is in conformity with the FTIR result. Electrostatic attraction also contributed to the adsorption, electron-negative phosphate was attracted by the positive charge of the surface and protonation of hydroxyl groups occurred until the positive charge was neutralized completely by phosphate, this also explains why the adsorption capacity increases as the metal ratio decreases (Hu *et al.* 2018). Table 6 demonstrates that the Mg_2Al-NO_3 LDH shows a better performance for the phosphate adsorption compared with other adsorbents.

Table 6 | Comparison study for the adsorption of phosphate by Mg_2Al-NO_3 LDH with other adsorbents

Adsorbent	Adsorption capacity (mg/g)	Reference
Mg-Al/biochar LDH	81.83	Li *et al.* (2016a)
ZnAl-PMA-LDH	64.8	Yu *et al.* (2015)
CuAl/CF-LDH	100	Hu *et al.* (2018)
La doping magnetic graphene	116.28	Rashidi Nodeh *et al.* (2017)
Zn_{3G}-Al	148.34	Hatami *et al.* (2018)
CMK-3@Mg-Al LDH	171	Yin *et al.* (2018)
Fe-Al hydroxides	51.8	Wang *et al.* (2013)
Mg-Al LDH	64.2	Khitous *et al.* (2016)
Titania/GO	33.11	Sakulpaisan *et al.* (2016)
Lanthanum hydroxides	107.5	Xie *et al.* (2014)
Mg_2Al-NO_3 LDH	185.86	This work

CONCLUSIONS

Layered double hydroxides with different Mg/Al ratios were prepared with nitrate to removal the phosphate from aqueous solution. XRD, SEM, and TEM analysis exhibited that the prepared samples have typical characteristic reflections and multilayer structure. The pseudo-second-order kinetic model is a better fit to the adsorption process indicating that

chemisorption is the crucial step of adsorption. Thermodynamic and isotherm studies showed that the adsorption process is endothermic and spontaneous in nature. The results of desorption experiments indicated that the desorption rate of all the LDHs can be higher than 95% and there is slight desorption hysteresis. The metal molar ratio had a significant effect on the adsorption capacity of LDHs, and the maximum adsorption capacity is 185.86 mg-KH_2PO_4/g for Mg_2Al-NO_3 LDH, which also has an excellent performance in reducing phosphate concentration in aqueous solution, indicating that the Mg_2Al-NO_3 adsorbent can effectively remove phosphate in the aqueous solution and has a promising industrial application prospect.

ACKNOWLEDGEMENTS

The research is part of the research project (2019YFC906400) supported by the Chinese Research Academy of Environmental Sciences.

DATA AVAILABILITY STATEMENT

All relevant data are included in the paper or its Supplementary Information.

REFERENCES

Abdul-Hameed, H. & Al Juboury, M. 2020 MgFe-doubled layers hydroxide intercalated with low cost local adsorbent using for removal of lead from aqueous solution. *J. Water L. Dev.* **45**, 10–18.

Abukhadra, M. R. & Mostafa, M. 2019 Effective decontamination of phosphate and ammonium utilizing novel muscovite/phillipsite composite; equilibrium investigation and realistic application. *Sci. Total Environ.* **667**, 101–111.

Abukhadra, M. R., Adlii, A., El-Sherbeeny, A. M., Ahmed Soliman, A. T. & Abd Elgawad, A. E. E. 2020a Promoting the decontamination of different types of water pollutants (Cd2 + , safranin dye, and phosphate) using a novel structure of exfoliated bentonite admixed with cellulose nanofiber. *J. Environ. Manage.* **273**, 111130.

Abukhadra, M. R., Ali, S. M., Nasr, E. A., Mahmoud, H. A. A. & Awwad, E. M. 2020b Effective sequestration of phosphate and ammonium ions by the bentonite/zeolite Na–P composite as a simple technique to control the eutrophication phenomenon: realistic studies. *ACS Omega* **5**, 14656–14668.

Adeola, A. O. & Forbes, P. B. C. 2020 Optimization of the sorption of selected polycyclic aromatic hydrocarbons by regenerable graphene wool. *Water Sci. Technol.* **80**, 1931–1943.

Alshameri, A., Yan, C. & Lei, X. 2014 Enhancement of phosphate removal from water by TiO_2/Yemeni natural zeolite: preparation, characterization and thermodynamic. *Microporous Mesoporous Mater.* **196**, 145–157.

Bao, S., Shi, Y., Zhang, Y., He, L., Yu, W., Chen, Z., Wu, Y. & Li, L. 2020 Study on the efficient removal of azo dyes by heterogeneous photo-Fenton process with 3D flower-like layered double hydroxide. *Water Sci. Technol.* **81**, 2368–2380.

Dewangan, N., Hui, W. M., Jayaprakash, S., Bawah, A.-R., Poerjoto, A. J., Jie, T., Jangam, A., Hidajat, K. & Kawi, S. 2020 Recent progress on layered double hydroxide (LDH) derived metal-based catalysts for CO_2 conversion to valuable chemicals. *Catal. Today* **356**, 490–513.

Everaert, M., Warrinnier, R., Baken, S., Gustafsson, J., De Vos, D. & Smolders, E. 2016 Phosphate-exchanged Mg-Al layered double hydroxides: a new slow release phosphate fertilizer. *ACS Sustainable Chem. Eng.* **4**, 4280–4287.

Hatami, H., Fotovat, A. & Halajnia, A. 2018 Comparison of adsorption and desorption of phosphate on synthesized Zn-Al LDH by two methods in a simulated soil solution. *Appl. Clay Sci.* **152**, 333–341.

Hu, F., Wang, M., Peng, X., Qiu, F., Zhang, T., Dai, H., Liu, Z. & Cao, Z. 2018 High-efficient adsorption of phosphates from water by hierarchical CuAl/biomass carbon fiber layered double hydroxide. *Colloids Surfaces A Physicochem. Eng. Asp.* **555**, 314–323.

Juboury, M. F. A. 2019 Using of activated carbon derived from agriculture waste coating by layered double hydroxide for copper adsorption. *Iraqi Journal of Agricultural Science.* **50** (5), 1446–1454.

Khitous, M., Salem, Z. & Halliche, D. 2016 Removal of phosphate from industrial wastewater using uncalcined MgAl-NO3 layered double hydroxide: batch study and modeling. *Desalin. Water Treat.* **57**, 15920–15931.

Kong, L., Tian, Y., Wang, Y., Li, N., Liu, Y., Pang, Z., Huang, X., Li, M., Zhang, J. & Zuo, W. 2019 Periclase-induced generation of flowerlike clay-based layered double hydroxides: a highly efficient phosphate scavenger and solid-phase fertilizer. *Chem. Eng. J.* **359**, 902–913.

Lalley, J., Han, C., Li, X., Dionysiou, D. D. & Nadagouda, M. N. 2016 Phosphate adsorption using modified iron oxide-based sorbents in lake water: kinetics, equilibrium, and column tests. *Chem. Eng. J.* **284**, 1386–1396.

Law, Y., Kirkegaard, R. H., Cokro, A. A., Liu, X., Arumugam, K., Xie, C., Stokholm-Bjerregaard, M., Drautz-Moses, D. I., Nielsen, P. H., Wuertz, S. & Williams, R. B. H. 2016 Integrative microbial community analysis reveals full-scale enhanced biological phosphorus removal under tropical conditions. *Sci. Rep.* **6**, 25719.

Li, R., Wang, J. J., Zhou, B., Awasthi, M. K., Ali, A., Zhang, Z., Gaston, L. A., Lahori, A. H. & Mahar, A. 2016a Enhancing phosphate adsorption by Mg/Al layered double hydroxide functionalized biochar with different Mg/Al ratios. *Sci. Total Environ.* **559**, 121–129.

Li, W., Zeng, L., Kang, Y., Zhang, Q., Luo, J. & Guo, X. 2016b A solid waste, crashed autoclaved aerated concrete, as a

crystalline nucleus for the removal of low concentration of phosphate. *Desalin. Water Treat.* **57**, 14169–14177.

Liu, J., Wu, P., Li, S., Chen, M., Cai, W., Zou, D., Zhu, N. & Dang, Z. 2019 Synergistic deep removal of As(III) and Cd(II) by a calcined multifunctional MgZnFe-CO_3 layered double hydroxide: photooxidation, precipitation and adsorption. *Chemosphere* **225**, 115–125.

Mohamed, F., Abukhadra, M. R. & Shaban, M. 2018 Removal of safranin dye from water using polypyrrole nanofiber/Zn-Fe layered double hydroxide nanocomposite (Ppy NF/Zn-Fe LDH) of enhanced adsorption and photocatalytic properties. *Sci. Total Environ* **640–641**, 352–363.

Rashidi Nodeh, H., Sereshti, H., Zamiri Afsharian, E. & Nouri, N. 2017 Enhanced removal of phosphate and nitrate ions from aqueous media using nanosized lanthanum hydrous doped on magnetic graphene nanocomposite. *J. Environ. Manage.* **197**, 265–274.

Sakulpaisan, S., Vongsetskul, T., Reamouppaturm, S., Luangkachao, J., Tantirungrotechai, J. & Tangboriboonrat, P. 2016 Titania-functionalized graphene oxide for an efficient adsorptive removal of phosphate ions. *J. Environ. Manage.* **167**, 99–104.

Santos, A., Arim, A., Lopes, D., Ferreira, L. & Quina, M. 2019 Recovery of phosphate from aqueous solutions using calcined eggshell as an eco-friendly adsorbent. *J. Environ. Manage.* **238**, 451–459.

Shi, Z., Wang, Y., Sun, S., Zhang, C. & Wang, H. 2020 Removal of methylene blue from aqueous solution using Mg-Fe, Zn-Fe, Mn-Fe layered double hydroxide. *Water Sci. Technol.* **81**, 2522–2532.

Valsami-Jones, E. 2005 *Phosphorus in Environmental Technology: Principles and Applications*. Water Intell. IWA Publishing, London, UK.

Wang, X.-H., Liu, F., Lu, L., Yang, S., Zhao, Y., Sun, L.-B. & Wang, S.-G. 2013 Individual and competitive adsorption of Cr(VI) and phosphate onto synthetic Fe-Al hydroxides. *Colloids Surfaces A Physicochem. Eng. Asp.* **423**, 42–49.

Xie, J., Wang, Z., Lu, S., Wu, D., Zhang, Z. & Kong, H. 2014 Removal and recovery of phosphate from water by lanthanum hydroxide materials. *Chem. Eng. J.* **254**, 163–170.

Yan, H., Chen, Q., Liu, J., Feng, Y. & Shih, K. 2018 Phosphorus recovery through adsorption by layered double hydroxide nano-composites and transfer into a struvite-like fertilizer. *Water Res.* **145**, 721–730.

Yin, L., Hu, Y., Ma, R., Hu, B., Yu, Z., Hayat, T., Alsaedi, A. & Wang, X. 2018 Smart construction of mesoporous carbon templated hierarchical Mg-Al and Ni-Al layered double hydroxides for remarkably enhanced U(VI) management. *Chem. Eng. J.* **359**, 1550–1562.

Yu, Q., Zheng, Y., Wang, Y., Shen, L., Wang, H., Zheng, Y., He, N. & Li, Q. 2015 Highly selective adsorption of phosphate by pyromellitic acid intercalated ZnAl-LDHs: assembling hydrogen bond acceptor sites. *Chem. Eng. J.* **260**, 809–817.

Zhang, L., Zhou, Q., Liu, J., Chang, N., Wan, L. & Chen, J. 2012a Phosphate adsorption on lanthanum hydroxide-doped activated carbon fiber. *Chem. Eng. J.* **185–186**, 160–167.

Zhang, M., Gao, B., Yao, Y., Xue, Y. & Inyang, M. 2012b Synthesis of porous MgO-biochar nanocomposites for removal of phosphate and nitrate from aqueous solutions. *Chem. Eng. J.* **210**, 26–32.

Zhang, M., Gao, B., Yao, Y. & Inyang, M. 2013 Phosphate removal ability of biochar/MgAl-LDH ultra-fine composites prepared by liquid-phase deposition. *Chemosphere* **92**, 1042–1047.

Zhang, Q., Ji, F., Zhao, T., Shen, Q., Fang, D., Kuang, L., Jiang, L. & Ding, S. 2019 Systematic screening of layered double hydroxides for phosphate removal and mechanism insight. *Appl. Clay Sci.* **174**, 159–169.

Zhao, S., Meng, Z., Fan, X., Jing, R., Yang, J., Shao, Y., Liu, X., Wu, M., Zhang, Q. & Liu, A. 2020 Removal of heavy metals from soil by vermiculite supported layered double hydroxides with three-dimensional hierarchical structure. *Chem. Eng. J.* **390**, 124554.

First received 17 September 2020; accepted in revised form 13 November 2020. Available online 27 November 2020